Evidence for Nonlinear Gluon Effects in QCD and their A Dependence at STAR

M. S. Abdallah,[5] B. E. Aboona,[55] J. Adam,[6] L. Adamczyk,[2] J. R. Adams,[39] J. K. Adkins,[30] G. Agakishiev,[28] I. Aggarwal,[41] M. M. Aggarwal,[41] Z. Ahammed,[60] I. Alekseev,[3,35] D. M. Anderson,[55] A. Aparin,[28] E. C. Aschenauer,[6] M. U. Ashraf,[11] F. G. Atetalla,[29] A. Attri,[41] G. S. Averichev,[28] V. Bairathi,[53] W. Baker,[10] J. G. Ball Cap,[20] K. Barish,[10] A. Behera,[52] R. Bellwied,[20] P. Bhagat,[27] A. Bhasin,[27] J. Bielcik,[14] J. Bielcikova,[38] I. G. Bordyuzhin,[3] J. D. Brandenburg,[6] A. V. Brandin,[35] I. Bunzarov,[28] X. Z. Cai,[50] H. Caines,[63] M. Calderón de la Barca Sánchez,[8] D. Cebra,[8] I. Chakaberia,[31,6] P. Chaloupka,[14] B. K. Chan,[9] F-H. Chang,[37] Z. Chang,[6] N. Chankova-Bunzarova,[28] A. Chatterjee,[11] S. Chattopadhyay,[60] D. Chen,[10] J. Chen,[49] J. H. Chen,[18] X. Chen,[48] Z. Chen,[49] J. Cheng,[57] M. Chevalier,[10] S. Choudhury,[18] W. Christie,[6] X. Chu,[6] H. J. Crawford,[7] M. Csanád,[16] M. Daugherity,[1] T. G. Dedovich,[28] I. M. Deppner,[19] A. A. Derevschikov,[43] A. Dhamija,[41] L. Di Carlo,[62] L. Didenko,[6] P. Dixit,[22] X. Dong,[31] J. L. Drachenberg,[1] E. Duckworth,[29] J. C. Dunlop,[6] N. Elsey,[62] J. Engelage,[7] G. Eppley,[45] S. Esumi,[58] O. Evdokimov,[12] A. Ewigleben,[32] O. Eyser,[6] R. Fatemi,[30] F. M. Fawzi,[5] S. Fazio,[6] P. Federic,[38] J. Fedorisin,[28] C. J. Feng,[37] Y. Feng,[44] P. Filip,[28] E. Finch,[51] Y. Fisyak,[6] A. Francisco,[63] C. Fu,[11] L. Fulek,[2] C. A. Gagliardi,[55] T. Galatyuk,[15] F. Geurts,[45] N. Ghimire,[54] A. Gibson,[59] K. Gopal,[23] X. Gou,[49] D. Grosnick,[59] A. Gupta,[27] W. Guryn,[6] A. I. Hamad,[29] A. Hamed,[5] Y. Han,[45] S. Harabasz,[15] M. D. Harasty,[8] J. W. Harris,[63] H. Harrison,[30] S. He,[11] W. He,[18] X. H. He,[26] Y. He,[49] S. Heppelmann,[8] S. Heppelmann,[42] N. Herrmann,[19] E. Hoffman,[20] L. Holub,[14] Y. Hu,[18] H. Huang,[37] H. Z. Huang,[9] S. L. Huang,[52] T. Huang,[37] X. Huang,[57] Y. Huang,[57] T. J. Humanic,[39] G. Igo,[9,*] D. Isenhower,[1] W. W. Jacobs,[25] C. Jena,[23] A. Jentsch,[6] Y. Ji,[31] J. Jia,[6,52] K. Jiang,[48] X. Ju,[48] E. G. Judd,[7] S. Kabana,[53] M. L. Kabir,[10] S. Kagamaster,[32] D. Kalinkin,[25,6] K. Kang,[57] D. Kapukchyan,[10] K. Kauder,[6] H. W. Ke,[6] D. Keane,[29] A. Kechechyan,[28] M. Kelsey,[62] Y. V. Khyzhniak,[35] D. P. Kikoła,[61] C. Kim,[10] B. Kimelman,[8] D. Kincses,[16] I. Kisel,[17] A. Kiselev,[6] A. G. Knospe,[32] H. S. Ko,[31] L. Kochenda,[35] L. K. Kosarzewski,[14] L. Kramarik,[14] P. Kravtsov,[35] L. Kumar,[41] S. Kumar,[26] R. Kunnawalkam Elayavalli,[63] J. H. Kwasizur,[25] R. Lacey,[52] S. Lan,[11] J. M. Landgraf,[6] J. Lauret,[6] A. Lebedev,[6] R. Lednicky,[28,38] J. H. Lee,[6] Y. H. Leung,[31] N. Lewis,[6] C. Li,[49] C. Li,[48] W. Li,[45] X. Li,[48] Y. Li,[57] X. Liang,[10] Y. Liang,[29] R. Licenik,[38] T. Lin,[49] Y. Lin,[11] M. A. Lisa,[39] F. Liu,[11] H. Liu,[25] H. Liu,[11] P. Liu,[52] T. Liu,[63] X. Liu,[39] Y. Liu,[55] Z. Liu,[48] T. Ljubicic,[6] W. J. Llope,[62] R. S. Longacre,[6] E. Loyd,[10] N. S. Lukow,[54] X. F. Luo,[11] L. Ma,[18] R. Ma,[6] Y. G. Ma,[18] N. Magdy,[12] D. Mallick,[36] S. Margetis,[29] C. Markert,[56] H. S. Matis,[31] J. A. Mazer,[46] N. G. Minaev,[43] S. Mioduszewski,[55] B. Mohanty,[36] M. M. Mondal,[52] I. Mooney,[62] D. A. Morozov,[43] A. Mukherjee,[16] M. Nagy,[16] J. D. Nam,[54] Md. Nasim,[22] K. Nayak,[11] D. Neff,[9] J. M. Nelson,[7] D. B. Nemes,[63] M. Nie,[49] G. Nigmatkulov,[35] T. Niida,[58] R. Nishitani,[58] L. V. Nogach,[43] T. Nonaka,[58] A. S. Nunes,[6] G. Odyniec,[31] A. Ogawa,[6] S. Oh,[31] V. A. Okorokov,[35] B. S. Page,[6] R. Pak,[6] J. Pan,[55] A. Pandav,[36] A. K. Pandey,[58] Y. Panebratsev,[28] P. Parfenov,[35] B. Pawlik,[40] D. Pawlowska,[61] C. Perkins,[7] L. Pinsky,[20] R. L. Pintér,[16] J. Pluta,[61] B. R. Pokhrel,[54] G. Ponimatkin,[38] J. Porter,[31] M. Posik,[54] V. Prozorova,[14] N. K. Pruthi,[41] M. Przybycien,[2] J. Putschke,[62] H. Qiu,[26] A. Quintero,[54] C. Racz,[10] S. K. Radhakrishnan,[29] N. Raha,[62] R. L. Ray,[56] R. Reed,[32] H. G. Ritter,[31] M. Robotkova,[38] O. V. Rogachevskiy,[28] J. L. Romero,[8] D. Roy,[46] L. Ruan,[6] J. Rusnak,[38] A. K. Sahoo,[22] N. R. Sahoo,[49] H. Sako,[58] S. Salur,[46] J. Sandweiss,[63,*] S. Sato,[58] W. B. Schmidke,[6] N. Schmitz,[33] B. R. Schweid,[52] F. Seck,[15] J. Seger,[13] M. Sergeeva,[9] R. Seto,[10] P. Seyboth,[33] N. Shah,[24] E. Shahaliev,[28] P. V. Shanmuganathan,[6] M. Shao,[48] T. Shao,[18] A. I. Sheikh,[29] D. Y. Shen,[18] S. S. Shi,[11] Y. Shi,[49] Q. Y. Shou,[18] E. P. Sichtermann,[31] R. Sikora,[2] M. Simko,[38] J. Singh,[41] S. Singha,[26] M. J. Skoby,[44] N. Smirnov,[63] Y. Söhngen,[19] W. Solyst,[25] P. Sorensen,[6] H. M. Spinka,[4,*] B. Srivastava,[44] T. D. S. Stanislaus,[59] M. Stefaniak,[61] D. J. Stewart,[63] M. Strikhanov,[35] B. Stringfellow,[44] A. A. P. Suaide,[47] M. Sumbera,[38] B. Summa,[42] X. M. Sun,[11] X. Sun,[12] Y. Sun,[48] Y. Sun,[21] B. Surrow,[54] D. N. Svirida,[3] Z. W. Sweger,[8] P. Szymanski,[61] A. H. Tang,[6] Z. Tang,[48] A. Taranenko,[35] T. Tarnowsky,[34] J. H. Thomas,[31] A. R. Timmins,[20] D. Tlusty,[13] T. Todoroki,[58] M. Tokarev,[28] C. A. Tomkiel,[32] S. Trentalange,[9] R. E. Tribble,[55] P. Tribedy,[6] S. K. Tripathy,[16] T. Truhlar,[14] B. A. Trzeciak,[14] O. D. Tsai,[9] Z. Tu,[6] T. Ullrich,[6] D. G. Underwood,[4,59] I. Upsal,[45] G. Van Buren,[6] J. Vanek,[38] A. N. Vasiliev,[43] I. Vassiliev,[17] V. Verkest,[62] F. Videbæk,[6] S. Vokal,[28] S. A. Voloshin,[62] F. Wang,[44] G. Wang,[9] J. S. Wang,[21] P. Wang,[48] X. Wang,[49] Y. Wang,[11] Y. Wang,[57] Z. Wang,[49] J. C. Webb,[6] P. C. Weidenkaff,[19] L. Wen,[9] G. D. Westfall,[34] H. Wieman,[31] S. W. Wissink,[25] J. Wu,[11] J. Wu,[26] Y. Wu,[10] B. Xi,[50] Z. G. Xiao,[57] G. Xie,[31] W. Xie,[44] H. Xu,[21] N. Xu,[31] Q. H. Xu,[49] Y. Xu,[49] Z. Xu,[6] Z. Xu,[9] G. Yan,[49] C. Yang,[49] Q. Yang,[49] S. Yang,[45] Y. Yang,[37] Z. Ye,[45] Z. Ye,[12] L. Yi,[49] K. Yip,[6] Y. Yu,[49] H. Zbroszczyk,[61] W. Zha,[48] C. Zhang,[52] D. Zhang,[11] J. Zhang,[49] S. Zhang,[12] S. Zhang,[18] X. P. Zhang,[57] Y. Zhang,[26] Y. Zhang,[48] Y. Zhang,[11]

Z. J. Zhang,[37] Z. Zhang,[6] Z. Zhang,[12] J. Zhao,[44] C. Zhou,[18] Y. Zhou,[11] X. Zhu,[57] M. Zurek,[4] and M. Zyzak[17]
(STAR Collaboration)

[1]*Abilene Christian University, Abilene, Texas 79699*
[2]*AGH University of Science and Technology, FPACS, Cracow 30-059, Poland*
[3]*Alikhanov Institute for Theoretical and Experimental Physics NRC "Kurchatov Institute", Moscow 117218, Russia*
[4]*Argonne National Laboratory, Argonne, Illinois 60439*
[5]*American University of Cairo, New Cairo 11835, New Cairo, Egypt*
[6]*Brookhaven National Laboratory, Upton, New York 11973*
[7]*University of California, Berkeley, California 94720*
[8]*University of California, Davis, California 95616*
[9]*University of California, Los Angeles, California 90095*
[10]*University of California, Riverside, California 92521*
[11]*Central China Normal University, Wuhan, Hubei 430079*
[12]*University of Illinois at Chicago, Chicago, Illinois 60607*
[13]*Creighton University, Omaha, Nebraska 68178*
[14]*Czech Technical University in Prague, FNSPE, Prague 115 19, Czech Republic*
[15]*Technische Universität Darmstadt, Darmstadt 64289, Germany*
[16]*ELTE Eötvös Loránd University, Budapest, Hungary H-1117*
[17]*Frankfurt Institute for Advanced Studies FIAS, Frankfurt 60438, Germany*
[18]*Fudan University, Shanghai, 200433*
[19]*University of Heidelberg, Heidelberg 69120, Germany*
[20]*University of Houston, Houston, Texas 77204*
[21]*Huzhou University, Huzhou, Zhejiang 313000*
[22]*Indian Institute of Science Education and Research (IISER), Berhampur 760010 , India*
[23]*Indian Institute of Science Education and Research (IISER) Tirupati, Tirupati 517507, India*
[24]*Indian Institute Technology, Patna, Bihar 801106, India*
[25]*Indiana University, Bloomington, Indiana 47408*
[26]*Institute of Modern Physics, Chinese Academy of Sciences, Lanzhou, Gansu 730000*
[27]*University of Jammu, Jammu 180001, India*
[28]*Joint Institute for Nuclear Research, Dubna 141 980, Russia*
[29]*Kent State University, Kent, Ohio 44242*
[30]*University of Kentucky, Lexington, Kentucky 40506-0055*
[31]*Lawrence Berkeley National Laboratory, Berkeley, California 94720*
[32]*Lehigh University, Bethlehem, Pennsylvania 18015*
[33]*Max-Planck-Institut für Physik, Munich 80805, Germany*
[34]*Michigan State University, East Lansing, Michigan 48824*
[35]*National Research Nuclear University MEPhI, Moscow 115409, Russia*
[36]*National Institute of Science Education and Research, HBNI, Jatni 752050, India*
[37]*National Cheng Kung University, Tainan 70101*
[38]*Nuclear Physics Institute of the CAS, Rez 250 68, Czech Republic*
[39]*Ohio State University, Columbus, Ohio 43210*
[40]*Institute of Nuclear Physics PAN, Cracow 31-342, Poland*
[41]*Panjab University, Chandigarh 160014, India*
[42]*Pennsylvania State University, University Park, Pennsylvania 16802*
[43]*NRC "Kurchatov Institute", Institute of High Energy Physics, Protvino 142281, Russia*
[44]*Purdue University, West Lafayette, Indiana 47907*
[45]*Rice University, Houston, Texas 77251*
[46]*Rutgers University, Piscataway, New Jersey 08854*
[47]*Universidade de São Paulo, São Paulo, Brazil 05314-970*
[48]*University of Science and Technology of China, Hefei, Anhui 230026*
[49]*Shandong University, Qingdao, Shandong 266237*
[50]*Shanghai Institute of Applied Physics, Chinese Academy of Sciences, Shanghai 201800*
[51]*Southern Connecticut State University, New Haven, Connecticut 06515*
[52]*State University of New York, Stony Brook, New York 11794*
[53]*Instituto de Alta Investigación, Universidad de Tarapacá, Arica 1000000, Chile*
[54]*Temple University, Philadelphia, Pennsylvania 19122*
[55]*Texas A&M University, College Station, Texas 77843*
[56]*University of Texas, Austin, Texas 78712*
[57]*Tsinghua University, Beijing 100084*
[58]*University of Tsukuba, Tsukuba, Ibaraki 305-8571, Japan*
[59]*Valparaiso University, Valparaiso, Indiana 46383*
[60]*Variable Energy Cyclotron Centre, Kolkata 700064, India*
[61]*Warsaw University of Technology, Warsaw 00-661, Poland*

[62] *Wayne State University, Detroit, Michigan 48201*
[63] *Yale University, New Haven, Connecticut 06520*

The STAR Collaboration reports measurements of back-to-back azimuthal correlations of di-π^0s produced at forward pseudorapidities ($2.6 < \eta < 4.0$) in p+p, p+Al, and p+Au collisions at a center-of-mass energy of 200 GeV. We observe a clear suppression of the correlated yields of back-to-back π^0 pairs in p+Al and p+Au collisions compared to the p+p data. The observed suppression of back-to-back pairs as a function of event activity and transverse momentum suggests nonlinear gluon dynamics arising at high parton densities. The larger suppression found in p+Au relative to p+Al collisions exhibits a dependence of the saturation scale, Q_s^2, on the mass number, A. The suppression in high-activity p+Au collisions is consistent with theoretical predictions including gluon saturation effects.

The quest to understand quantum chromodynamics (QCD) processes in cold nuclear matter has in the last years revolved around the following questions: Can we experimentally find evidence for a novel universal regime of nonlinear QCD dynamics in nuclei? What is the role of saturated strong gluon fields? And what are the degrees of freedom in this high gluon density regime? These questions have motivated and continue to motivate theoretical efforts and experiments at facilities worldwide.

Collisions between hadronic systems, *i.e.*, p+A and d+A at the Relativistic Heavy Ion Collider (RHIC) provide a window to the parton distributions of nuclei at small momentum fraction x (down to 10^{-3}). Several RHIC measurements have shown that, at forward pseudorapidities (deuteron going direction), the hadron yields are suppressed in d+Au collisions relative to p+p collisions in inclusive productions [1–4] and di-hadron correlations [4, 5]. The mechanisms leading to the suppression are not firmly established. The density of gluons in nucleons and nuclei increases at low x due to gluon splitting. At a sufficiently small value of x, yet to be determined by experiments, the splitting is expected to be balanced by gluon recombination [6, 7]. The resulting gluon saturation [8–15] is one of the possible explanations for the suppression of forward hadron (jet) production. Initial- and final-state multiple scattering can determine the strength of the nuclear-induced transverse momentum imbalance for back-to-back particles [16–19]. Energy loss in the nuclear medium is also predicted to result in a significant suppression of forward hadron (jet) production. For d+A the contributions from double-parton interactions to the d+$A\to\pi^0\pi^0$X cross section are suggested as an alternative explanation for the suppression [20]. Therefore, it is important to make the same measurements in the theoretically and experimentally cleaner p+A collisions.

Back-to-back di-hadron azimuthal angle correlations have been proposed to be one of the most sensitive probes to directly access the underlying gluon dynamics involved in hard scatterings [21, 22]. At a given x, the density of gluons per unit transverse area is expected to be larger in nuclei than in nucleons; thus, nuclei provide a natural environment to study nonlinear gluon evolution [8]. Under the color glass condensate (CGC) framework [23–25], gluons from different nucleons are predicted to amplify the total transverse gluon density by a factor of $A^{1/3}$ for a nucleus with mass number A. One can parametrize the gluon distributions following the Golec-Biernat Wüsthoff (GBW) mode [26] with saturation scale $Q_s^2 \propto A^{1/3}Q_{s0}^2(x/x_0)^{-\lambda}$, where $Q_{s0} = 1$ GeV, $x_0 = 3.04\times10^{-4}$, and $\lambda = 0.288$. The CGC framework predicts that at forward angles (large pseudorapidities) high x quarks and gluons in the nucleon interact coherently with gluons at low x in the nucleus [27]. As a result, the probability to observe the associated hadrons is expected to be suppressed in $p(d)$+A collisions compared to p+p, and an angular broadening of the back-to-back correlation of di-hadrons is predicted [28, 29].

In this Letter, we report measurements of back-to-back azimuthal correlations of di-π^0s in p+Al and p+Au relative to p+p collisions in the forward-pseudorapidity region ($2.6 < \eta < 4.0$) at $\sqrt{s_{\rm NN}} = 200$ GeV. If the suppression of correlation functions is observed in p+A collisions, the use of different ion beams provides the opportunity to test the CGC prediction of Q_s^2 dependence on A. The data were obtained from p+p, p+Al, and p+Au collisions in 2015 with the π^0s reconstructed from photons, which were identified with the STAR forward meson spectrometer (FMS).

The FMS is an electromagnetic calorimeter installed at the STAR experiment in the forward-pseudorapidity region [30]. It is 7 meters away from the nominal interaction point, facing the clockwise circulating RHIC proton beam, which makes the FMS response insensitive to the p, Al, and Au target beam remnants. The FMS is a highly-segmented octagonal shaped wall with a 40 cm × 40 cm square hole surrounding the beam pipe. It contains 1264 lead glass blocks of two different types and sizes. The 476 small cells from the inner portion each have dimensions of about 3.8 cm × 3.8 cm × 45 cm and collectively cover a pseudorapidity range from 3.3 to 4.0. The outer region surrounding the small cells is a set of 788 large cells, 5.8 cm × 5.8 cm × 60 cm in size, covering a pseudorapidity range from 2.6 to 3.3.

The collision events are triggered by the FMS itself, based on the transverse energy. The FMS board sum triggers [30], which demand that the energy sum in localized overlapping areas is above particular thresholds, are used in the analysis. The p+Al and p+Au sam-

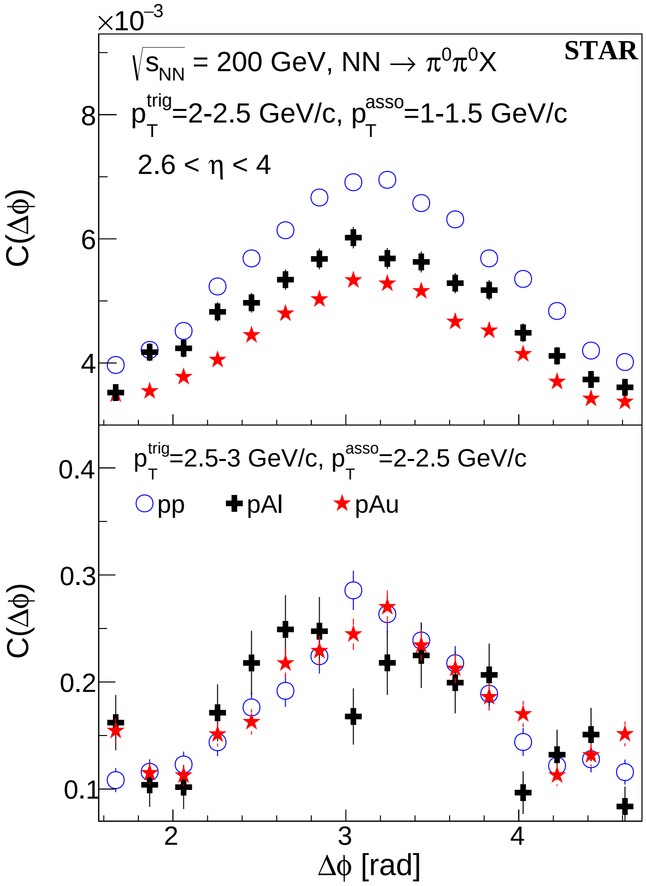

FIG. 1. (color online). Comparison of the correlation functions (corrected for nonuniform detector efficiency in ϕ; not corrected for the absolute detection efficiency) vs. azimuthal angle difference between forward ($2.6 < \eta < 4.0$) π^0s in p+p, p+Al, and p+Au collisions at $\sqrt{s_{\rm NN}} = 200$ GeV. Upper panel: the trigger π^0's p_T ($p_T^{\rm trig}$) = 2–2.5 GeV/c and the associated π^0's p_T ($p_T^{\rm asso}$) = 1–1.5 GeV/c; according to the fit described in the text, the area$\times 10^3$ (width) of the correlation in p+p, p+Al, and p+Au collisions are 5.67 ± 0.12 (0.68 ± 0.01), 4.15 ± 0.24 (0.68 ± 0.03), and 3.30 ± 0.07 (0.64 ± 0.01), respectively. Bottom panel: $p_T^{\rm trig} = 2.5$–3 GeV/c and $p_T^{\rm asso} = 2$–2.5 GeV/c; the area$\times 10^3$ (width) of the correlation in p+p, p+Al, and p+Au collisions are 0.18 ± 0.01 (0.47 ± 0.03), 0.13 ± 0.03 (0.51 ± 0.07), and 0.15 ± 0.01 (0.45 ± 0.03), respectively.

ples are separated into different event activity (E.A.) classes based on the energy deposited ($\Sigma E_{\rm BBC}$) in the backward (aluminum and gold going direction) inner sectors of the beam beam counter (BBC, $3.3 < -\eta < 5.0$), where $\Sigma E_{\rm BBC}$ in each event is the ADC sum from all 18 BBC tiles. The STAR BBC is a scintillator detector which measures minimum-ionizing particles [31]. Details on the E.A. selection can be found in the supplemental material [32]. To remove the beam background, the multiplicity at the Time of Flight detector ($|\eta| < 0.9$) [33] is required to be above 2 and the number of tiles firing at the backward BBC is above 0. The energy and transverse momentum, p_T, of the photon candidates are required to be above 1 GeV and 0.1 GeV/c, respectively. The energy asymmetry of π^0's photon components $|\frac{E_1 - E_2}{E_1 + E_2}|$ is required to be under 0.7 to reduce the combinatoric background which peaks near 1; this selection is commonly utilized in reconstructing π^0s with the FMS [34, 35]. The selected invariant mass range of the π^0 candidates is between 0.07 and 0.2 GeV/c^2.

The correlation function, $C(\Delta\phi)$, is defined as $C(\Delta\phi) = \frac{N_{\rm pair}(\Delta\phi)}{N_{\rm trig} \times \Delta\phi_{\rm bin}}$, where $N_{\rm pair}$ is the yield of the correlated trigger and associated π^0 pairs, $N_{\rm trig}$ is the trigger π^0 yield, $\Delta\phi$ is the azimuthal angle difference between the trigger π^0 and associated π^0, and $\Delta\phi_{\rm bin}$ is the bin width of $\Delta\phi$ distribution. In each pair, the trigger π^0 is the one with the higher p_T value, $p_T^{\rm trig}$, and the associated π^0 is the one with the lower p_T value, $p_T^{\rm asso}$. To remove the correlation induced by asymmetric detector effects, the measured correlation functions shown in this Letter are corrected through dividing them by the correlation functions computed for mixed events. $\Delta\phi$ distributions of two π^0s produced in different events are extracted from the ϕ distributions of the trigger π^0s and the associated π^0s. The correlation for mixed events is the $\Delta\phi$ distribution normalized by $N_{\rm bin}/N_{\rm pair}^{\rm mix}$, where $N_{\rm bin}$ is the number of bins in $\Delta\phi$ and $N_{\rm pair}^{\rm mix}$ is the number of π^0 pairs for mixed events. The correlations are not corrected for the absolute detection efficiency. The corrected correlation function is fitted from $\Delta\phi = -\pi/2$ to $\Delta\phi = 3\pi/2$ with two individual Gaussians at the near- ($\Delta\phi = 0$) and away-side ($\Delta\phi = \pi$) peak, together with a constant for the pedestal. The area of the away-side peak is the integral of the correlation function from $\Delta\phi = \pi/2$ to $\Delta\phi = 3\pi/2$ after pedestal subtraction, describing the back-to-back π^0 yields per trigger particle; the corresponding width is defined as the σ of the away-side peak according to the fit.

Figure 1 shows the comparison of $C(\Delta\phi)$ for forward back-to-back π^0 pairs observed in p+p, p+Al, and p+Au collisions at $\sqrt{s_{\rm NN}} = 200$ GeV. In the upper panel, in the low-p_T regime, a clear suppression is observed in p+A compared to the p+p data. The back-to-back π^0 yields per trigger in p+Au (p+Al) are suppressed by about a factor of 1.7 (1.4) with respect to p+p collisions. Larger suppression in p+Au relative to p+Al at the same collision energy supports an A dependence of Q_s^2 as predicted in references [23, 28]. The suppression decreases with increasing p_T of the π^0s. From the bottom panel of Fig. 1, the suppression is found to be weaker compared to the low-p_T range in p+Au collisions. The area, width, and pedestal in p+p, p+Al, and p+Au collisions with full di-π^0 p_T combinations can be found in the supplemental material [32]. The parton momentum fraction x with respect to the nucleon inside the nucleus is proportional to the p_T of the two π^0s; Q can be approximated as the average p_T of the two π^0s. Varying the gluon density in x and Q^2 can be achieved by changing the p_T of the two π^0s

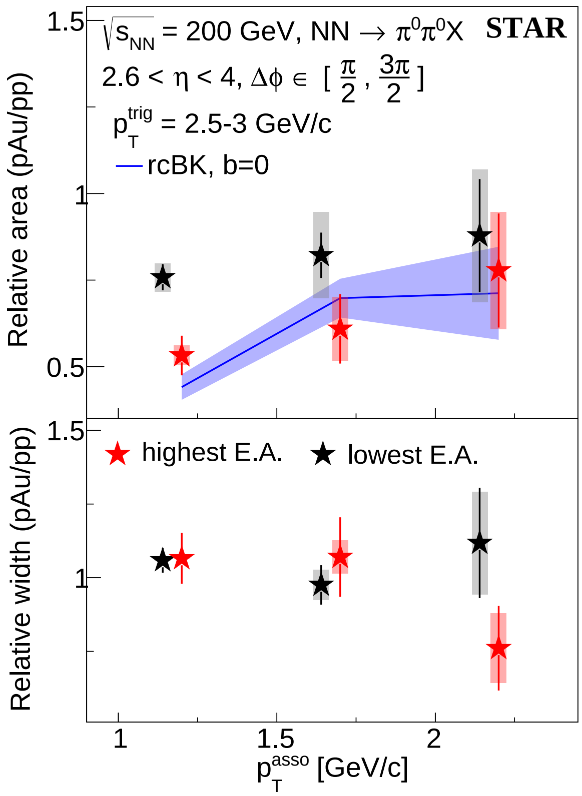

FIG. 2. (color online). Relative area (upper panel) and relative width (bottom panel) of back-to-back di-π^0 correlation at forward pseudorapidities ($2.6 < \eta < 4.0$) for different event activities (E.A.) in p+Au relative to p+p collisions for $p_T^{\rm trig} =$ 2.5−3 GeV/c as a function of $p_T^{\rm asso}$. The vertical bars indicate the statistical uncertainties and the vertical bands indicate the point-to-point systematic uncertainties. The width of the band is chosen for visual clarity and does not reflect uncertainty in $p_T^{\rm asso}$. The measured relative area for the highest E.A. is compared with theory predictions based on the rcBK model [36] at an impact parameter $b = 0$. The lowest E.A. points are slightly offset in $p_T^{\rm asso}$ for visual clarity.

at forward pseudorapidities. The low x and Q^2 regime where the gluon density is large and expected to be saturated, can be accessed by probing low-p_T π^0s; when p_T is high, x (Q^2) is not sufficiently small to reach the nonlinear regime. The simulated x and Q^2 distributions in p+p collisions can be found in the supplemental material [32].

In the upper (bottom) panel of Fig. 2, the relative area (width) of back-to-back di-π^0 correlations in p+Au with respect to p+p collisions is shown as a function of $p_T^{\rm asso}$ for the lowest and highest E.A.s. The area and width in p+p collisions are obtained without E.A. selection. The systematic uncertainties of area and width are estimated from nonuniform detector efficiency for each collision system as a function of ϕ. A data driven Monte Carlo method was performed bin by bin in p_T to determine the systematic uncertainties of the area and width. An input correlation, without detector effects, was sampled by two Gaussians at the near-/away-side peaks and a constant for pedestal. A correlation with detector effects included was obtained by weighting the ϕ distributions with the data and then a mixed-event correction was applied to the correlation. The difference between the input and the corrected correlations defines the estimated systematic uncertainties, which serves as a closure test. The systematic uncertainty depends on p_T and rarely depends on E.A. The systematic uncertainties of the relative area obtained at $p_T^{\rm asso} = 1{-}1.5$ GeV/c, 1.5−2 GeV/c, and 2−2.5 GeV/c are around 5%, 15%, and 22%, respectively, for $p_T^{\rm trig} = 2.5{-}3$ GeV/c. The corresponding systematic uncertainties of the relative width are 0.1%, 5%, and 16%.

Theoretical calculations[1] from Ref. [36] predict the area ratio of central p+Au collisions (impact parameter $b = 0$) relative to p+p collisions and are shown in the upper panel of Fig. 2. In this model, the gluon content of the saturated nuclear target is described with transverse-momentum-dependent (TMD) gluon distributions and the small-x evolution is calculated numerically by solving the nonlinear Balitsky-Kovchegov equation [40, 41] with running coupling corrections (rcBK). No comparison between the data and prediction of the width is made, since the model currently does not take into account soft gluon radiation as well as several other factors that affect the width. Agreement is found between the relative area from predictions and the data in the highest activity p+Au collisions.

In the upper panel of Fig. 2, at low $p_T^{\rm asso}$, the suppression in p+Au collisions becomes larger in high activity events compared to low activity events. In the bottom panel, the Gaussian widths of the correlated peaks remain the same between p+p and p+Au at various E.A.s, *i.e.*, the broadening predicted in the CGC framework in Ref. [28, 29] is not observed. This observation agrees with a similar measurement in d+Au collisions by the PHENIX experiment [5]. The pedestals from p+p and p+A do not vary (see supplemental material [32]), which can provide information on multiple parton interactions in d+Au collisions where the measured pedestal is 2-3 times higher than in p+p [5]. The area, width, and pedestal for different E.A.s in p+Au collisions with full di-π^0 p_T combinations can be found in the supplemental material [32].

In Fig. 3, the back-to-back di-π^0 correlations measured in p+Al are compared with those in p+Au collisions for different E.A. bins. The results are obtained for low di-π^0 p_T ($p_T^{\rm trig} = 1.5{-}2$ GeV/c and $p_T^{\rm asso} = 1{-}1.5$ GeV/c) because of the limited statistics of the p+Al data. The tendency of enhanced suppression in high activity events is observed in p+Al data. The suppression for the highest

[1] Calculations are not compared with the data since Ref. [37] is for different collision systems and Refs. [38, 39] have no centrality dependence in p+Au collisions.

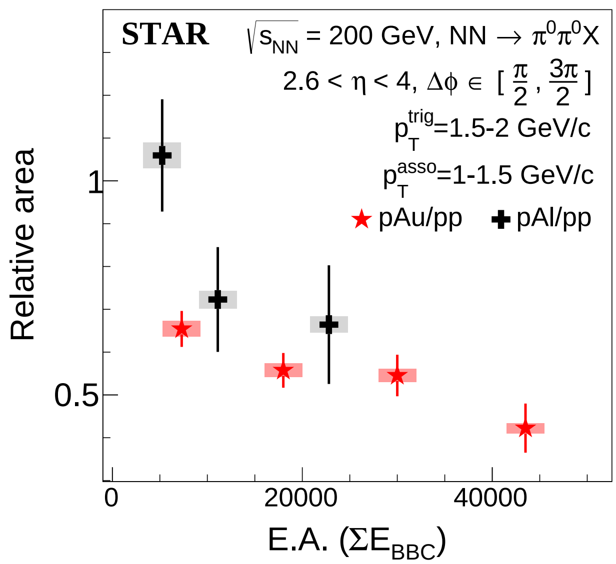

FIG. 3. (color online). Relative area of back-to-back di-π^0 correlations at forward pseudorapidities ($2.6 < \eta < 4.0$) for different event activity bins from p+Al and p+Au relative to p+p collisions for $p_T^{\rm trig} = 1.5{-}2$ GeV/c and $p_T^{\rm asso} = 1{-}1.5$ GeV/c. Around each data point the vertical bars indicate statistical uncertainties and the vertical bands indicate point-to-point systematic uncertainties. The width of the band is chosen for visibility and doesn't reflect uncertainties.

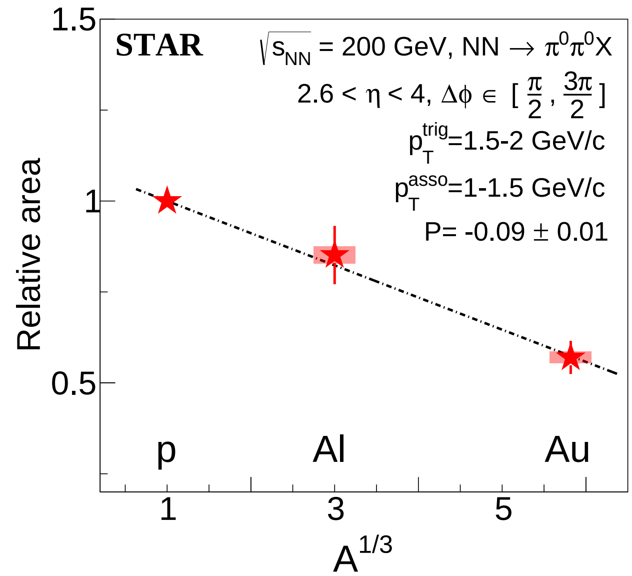

FIG. 4. (color online). Relative area of back-to-back di-π^0 correlations at forward pseudorapidities ($2.6 < \eta < 4.0$) in p+Au and p+Al relative to p+p collisions for $p_T^{\rm trig} = 1.5{-}2$ GeV/c and $p_T^{\rm asso} = 1{-}1.5$ GeV/c. The vertical bars for the Al and Au ratios indicate the statistical uncertainties and the vertical bands indicate the point-to-point systematic uncertainties. The horizontal width of the bands is chosen for visual clarity and does not reflect uncertainty. The data points are fitted by a linear function, whose slope (P) is found to be -0.09 ± 0.01.

E.A. compared to the lowest E.A. in p+Al and p+Au collisions has a significance of 2.0 and 3.1, respectively. Less suppression is found in p+Al compared to p+Au collisions, which is consistent with the results from p+Al and p+Au data at low p_T in the upper panel of Fig. 1.

The STAR experiment performed a unique measurement of the A-dependence in back-to-back di-π^0 correlations at forward pseudorapidities. The relative area in p+Au and p+Al with respect to p+p collisions is shown in Fig. 4 as a function of $A^{1/3}$; the systematic uncertainty is around 3% at $p_T^{\rm trig} = 1.5{-}2$ GeV/c and $p_T^{\rm asso} = 1{-}1.5$ GeV/c. The ratio for $A = 1$ has no uncertainty since the numerator and denominator are fully correlated. A specific p_T range probes the suppression in p+Au and p+Al collisions in the same x-Q^2 phase space. Therefore, the suppression is dominantly influenced by A according to the GBW model [26]. A linear dependence of the suppression as a function of $A^{1/3}$ is observed within the uncertainties in Fig. 4, the slope (P) is found to be -0.09 ± 0.01.

In summary, the measurements of azimuthal correlations of di-π^0s at forward pseudorapidities are performed using 2015 STAR 200 GeV p+p, p+Al, and p+Au data. Results of the back-to-back correlations are given as a function of p_T, with the trigger π^0 in the range of $1.5 < p_T^{\rm trig} < 5$ GeV/c and the associated π^0 in the range of $1 < p_T^{\rm asso} < 2.5$ GeV/c. A clear suppression of back-to-back yields is observed in p+A compared to p+p data, for pairs probing small x (and Q^2) with low p_T. The suppression is analyzed for various E.A. selections and found to be larger with higher E.A. The measured suppression in high E.A. p+Au collisions is consistent with the predictions calculated from the gluon saturation model. The present results are the first measurements of the A-dependence of this nuclear effect; the suppression is enhanced with higher A and scales with $A^{1/3}$. No increase in the width of the azimuthal angular correlation is seen within experimental uncertainties. The stable pedestal in p+A and p+p collisions provides opportunities to understand the contributions from multiple parton scatterings in d+A collisions.

We thank the RHIC Operations Group and RCF at BNL, the NERSC Center at LBNL, and the Open Science Grid consortium for providing resources and support. This work was supported in part by the Office of Nuclear Physics within the U.S. DOE Office of Science, the U.S. National Science Foundation, the Ministry of Education and Science of the Russian Federation, National Natural Science Foundation of China, Chinese Academy of Science, the Ministry of Science and Technology of China and the Chinese Ministry of Education, the Higher Education Sprout Project by Ministry of Education at NCKU, the National Research Foundation of Korea, Czech Science Foundation and Ministry of Education, Youth and Sports of the Czech Republic, Hungarian National Research, Development and Innovation Office, New National Excellency Programme of the Hungarian Ministry of Human Capacities, Department of Atomic Energy and Department of Science and Technology of the Government of India, the National Science Centre of Poland, the Ministry of Science, Education and Sports of the Republic of Croatia, RosAtom of Russia and German Bundesministerium für Bildung, Wissenschaft, Forschung and Technologie (BMBF), Helmholtz Association, Ministry of Education, Culture, Sports, Science, and Technology (MEXT) and Japan Society for the Promotion of Science (JSPS).

---

* Deceased

[1] I. Arsene et al. (BRAHMS), Phys. Rev. Lett. **91**, 072305 (2003), nucl-ex/0307003.
[2] I. Arsene et al. (BRAHMS), Phys. Rev. Lett. **93**, 242303 (2004), nucl-ex/0403005.
[3] S. S. Adler et al. (PHENIX), Phys. Rev. Lett. **94**, 082302 (2005), nucl-ex/0411054.
[4] J. Adams et al. (STAR), Phys. Rev. Lett. **97**, 152302 (2006), nucl-ex/0602011.
[5] A. Adare et al. (PHENIX), Phys. Rev. Lett. **107**, 172301 (2011), 1105.5112.
[6] A. H. Mueller and J.-w. Qiu, Nucl. Phys. B **268**, 427 (1986).
[7] R. C. Hwa, C. B. Yang, and R. J. Fries, Phys. Rev. C **71**, 024902 (2005), nucl-th/0410111.
[8] L. V. Gribov, E. M. Levin, and M. G. Ryskin, Phys. Rept. **100**, 1 (1983).
[9] N. Armesto, C. A. Salgado, and U. A. Wiedemann, Phys. Rev. Lett. **94**, 022002 (2005), hep-ph/0407018.
[10] F. Gelis, E. Iancu, J. Jalilian-Marian, and R. Venugopalan, Ann. Rev. Nucl. Part. Sci. **60**, 463 (2010), 1002.0333.
[11] J. L. Albacete and C. Marquet, Phys. Rev. Lett. **105**, 162301 (2010), 1005.4065.
[12] K. Tuchin, Nucl. Phys. A **846**, 83 (2010), 0912.5479.
[13] Y. V. Kovchegov and E. Levin, Quantum chromodynamics at high energy, vol. 33 (Cambridge University Press, 2012).
[14] J. Albacete and C. Marquet, Progress in Particle and Nuclear Physics **76**, 1 (2014), 1401.4866.
[15] A. Morreale and F. Salazar, Universe **7**, 312 (2021), 2108.08254.
[16] I. Vitev, Phys. Lett. B **562**, 36 (2003), nucl-th/0302002.
[17] I. Vitev, Phys. Rev. C **75**, 064906 (2007), hep-ph/0703002.
[18] L. Frankfurt and M. Strikman, Phys. Lett. B **645**, 412 (2007), nucl-th/0603049.
[19] Z.-B. Kang, I. Vitev, and H. Xing, Phys. Rev. D **85**, 054024 (2012), 1112.6021.
[20] M. Strikman and W. Vogelsang, Phys. Rev. D **83**, 034029 (2011), 1009.6123.
[21] C. Marquet, Nucl. Phys. A **796**, 41 (2007), 0708.0231.
[22] L. Zheng, E. C. Aschenauer, J. H. Lee, and B.-W. Xiao, Phys. Rev. D **89**, 074037 (2014), 1403.2413.
[23] L. D. McLerran and R. Venugopalan, Phys. Rev. D **49**, 2233 (1994), hep-ph/9309289.
[24] L. D. McLerran and R. Venugopalan, Phys. Rev. D **49**, 3352 (1994), hep-ph/9311205.
[25] E. Iancu, A. Leonidov, and L. McLerran (Springer, 2002), pp. 73–145.
[26] K. J. Golec-Biernat and M. Wusthoff, Phys. Rev. D **59**, 014017 (1998), hep-ph/9807513.
[27] V. Guzey, M. Strikman, and W. Vogelsang, Phys. Lett. B **603**, 173 (2004), hep-ph/0407201.
[28] D. Kharzeev, E. Levin, and L. McLerran, Nucl. Phys. A **748**, 627 (2005), hep-ph/0403271.
[29] C. Marquet, Nucl. Phys. A **796**, 41 (2007), 0708.0231.
[30] J. Adam et al. (STAR), Phys. Rev. D **98**, 032013 (2018), 1805.09745.
[31] C. A. Whitten (STAR), AIP Conf. Proc. **980**, 390 (2008).
[32] J. Adam et al. (STAR), Supplemental material of this Letter (2021).
[33] K. H. Ackermann et al. (STAR), Nucl. Instrum. Meth. A **499**, 624 (2003).
[34] J. Adam et al. (STAR), Phys. Rev. D **103**, 072005 (2021), 2012.07146.
[35] J. Adam et al. (STAR), Phys. Rev. D **103**, 092009 (2021), 2012.11428.
[36] J. L. Albacete, G. Giacalone, C. Marquet, and M. Matas, Phys. Rev. D **99**, 014002 (2019), 1805.05711.
[37] A. Stasto, B.-W. Xiao, and F. Yuan, Phys. Lett. B **716**, 430 (2012), 1109.1817.
[38] T. Lappi and H. Mantysaari, Nucl. Phys. A **908**, 51 (2013), 1209.2853.
[39] A. Stasto, S.-Y. Wei, B.-W. Xiao, and F. Yuan, Phys. Lett. B **784**, 301 (2018), 1805.05712.
[40] I. Balitsky, Nucl. Phys. B **463**, 99 (1996), hep-ph/9509348.
[41] Y. V. Kovchegov, Phys. Rev. D **60**, 034008 (1999), hep-ph/9901281.

SUPPLEMENTAL MATERIAL

Beam species	Event activity (E.A.)	ΣE_{BBC} range ($\times 10^3$)	Class
	Lowest	3-8	31%-60%
p+Al	Medium	8-15	60%-81%
	Highest	>15	81%-100%
	Lowest	3-12	15%-43%
p+Au	Medium low	12-24	43%-69%
	Medium high	24-36	69%-88%
	Highest	>36	88%-100%

TABLE I. Definition of the event activity classes in p+Al and p+Au collisions based on the energy deposited in the East BBC for the analyzed event samples.

p_T^{asso} [GeV/c]			p_T^{trig} [GeV/c]		Parameter
	1.5-2.0	2.0-2.5	2.5-3.0	3.0-5.0	
	4.51±0.15	5.67±0.12	5.34±0.11	5.58±0.11	Area$\times 10^3$
1.0-1.5	0.59±0.02	0.68±0.01	0.64±0.01	0.67±0.01	Width
	29.47±0.26	23.10±0.17	23.14±0.17	21.68±0.17	Pedestal$\times 10^3$
		1.03±0.03	0.91±0.03	1.09±0.04	Area$\times 10^3$
1.5-2.0		0.61±0.02	0.55±0.02	0.66±0.02	Width
		3.15±0.05	3.10±0.05	2.51±0.06	Pedestal$\times 10^3$
			0.18±0.01	0.23±0.02	Area$\times 10^3$
2.0-2.5			0.47±0.03	0.61±0.04	Width
			0.74±0.02	0.50±0.02	Pedestal$\times 10^3$

TABLE II. The area, width, and pedestal according to the fit of forward ($2.6 < \eta < 4.0$) back-to-back di-π^0 correlations in MinBias p+p collisions for various p_T ranges.

p_T^{asso} [GeV/c]			p_T^{trig} [GeV/c]		Parameter
	1.5-2.0	2.0-2.5	2.5-3.0	3.0-5.0	
	3.84±0.28	4.15±0.24	4.40±0.22	4.07±0.22	Area$\times 10^3$
1.0-1.5	0.60±0.04	0.68±0.03	0.67±0.03	0.70±0.03	Width
	27.30±0.48	21.84±0.36	20.25±0.34	19.05±0.33	Pedestal$\times 10^3$
		0.69±0.07	0.65±0.07	0.69±0.06	Area$\times 10^3$
1.5-2.0		0.53±0.04	0.60±0.05	0.59±0.04	Width
		3.77±0.01	2.92±0.11	2.65±0.09	Pedestal$\times 10^3$
			0.13±0.03	0.29±0.09	Area$\times 10^3$
2.0-2.5			0.51±0.07	0.96±0.19	Width
			0.79±0.05	0.42±0.11	Pedestal$\times 10^3$

TABLE III. The area, width, and pedestal according to the fit of forward ($2.6 < \eta < 4.0$) back-to-back di-π^0 correlations in MinBias p+Al collisions for various p_T ranges.

$p_T^{\rm asso}$ [GeV/c]	$p_T^{\rm trig}$ [GeV/c]				Parameter
	1.5-2.0	2.0-2.5	2.5-3.0	3.0-5.0	
1.0-1.5	2.57±0.08	3.30±0.07	3.55±0.09	3.17±0.09	Area×10^3
	0.49±0.01	0.64±0.01	0.65±0.01	0.64±0.01	Width
	25.68±0.15	20.46±0.11	19.33±0.14	18.54±0.13	Pedestal×10^3
1.5-2.0		0.76±0.03	0.65±0.03	0.75±0.04	Area×10^3
		0.62±0.02	0.55±0.02	0.71±0.03	Width
		3.26±0.04	3.09±0.05	2.56±0.06	Pedestal×10^3
2.0-2.5			0.15±0.01	0.18±0.02	Area×10^3
			0.45±0.03	0.71±0.07	Width
			0.81±0.02	0.63±0.03	Pedestal×10^3

TABLE IV. The area, width, and pedestal according to the fit of forward ($2.6 < \eta < 4.0$) back-to-back di-π^0 correlations in MinBias p+Au collisions for various p_T ranges.

$p_T^{\rm asso}$ [GeV/c]	$p_T^{\rm trig}$ [GeV/c]				Parameter
	1.5-2.0	2.0-2.5	2.5-3.0	3.0-5.0	
1.0-1.5	2.95±0.16	3.84±0.13	4.04±0.18	3.74±0.17	Area×10^3
	0.52±0.02	0.66±0.02	0.67±0.02	0.65±0.02	Width
	24.35±0.29	19.73±0.20	18.35±0.27	17.63±0.26	Pedestal×10^3
1.5-2.0		0.90±0.05	0.75±0.05	0.69±0.06	Area×10^3
		0.62±0.03	0.54±0.03	0.63±0.05	Width
		3.10±0.07	3.14±0.08	2.60±0.09	Pedestal×10^3
2.0-2.5			0.16±0.03	0.28±0.07	Area×10^3
			0.53±0.08	0.90±0.16	Width
			0.83±0.04	0.51±0.09	Pedestal×10^3

TABLE V. The area, width, and pedestal according to the fit of forward ($2.6 < \eta < 4.0$) back-to-back di-π^0 correlations in the lowest E.A. p+Au collisions for various p_T ranges.

$p_T^{\rm asso}$ [GeV/c]	$p_T^{\rm trig}$ [GeV/c]				Parameter
	1.5-2.0	2.0-2.5	2.5-3.0	3.0-5.0	
1.0-1.5	1.91±0.25	2.44±0.20	2.84±0.30	2.69±0.29	Area×10^3
	0.46±0.05	0.62±0.04	0.68±0.05	0.68±0.06	Width
	30.95±0.49	24.06±0.33	22.79±0.48	21.90±0.46	Pedestal×10^3
1.5-2.0		0.56±0.07	0.56±0.09	0.65±0.10	Area×10^3
		0.56±0.06	0.59±0.07	0.64±0.08	Width
		3.75±0.11	3.25±0.15	2.77±0.15	Pedestal×10^3
2.0-2.5			0.14±0.03	0.18±0.04	Area×10^3
			0.36±0.06	0.52±0.11	Width
			0.70±0.05	0.53±0.06	Pedestal×10^3

TABLE VI. The area, width, and pedestal according to the fit of forward ($2.6 < \eta < 4.0$) back-to-back di-π^0 correlations in the highest E.A. p+Au collisions for various p_T ranges.

E.A.	Area×10^3	Width	Pedestal×10^3
Lowest E.A.	4.78±0.57	0.65±0.06	24.38±0.93
Highest E.A.	3.00±0.62	0.51±0.09	37.16±1.17

TABLE VII. The area, width, and pedestal according to the fit of forward ($2.6 < \eta < 4.0$) back-to-back di-π^0 correlations in the lowest and highest E.A. p+Al collisions for $p_T^{\rm trig}$ = 1.5-2.0 GeV/c and $p_T^{\rm asso}$ = 1.0-1.5 GeV/c.

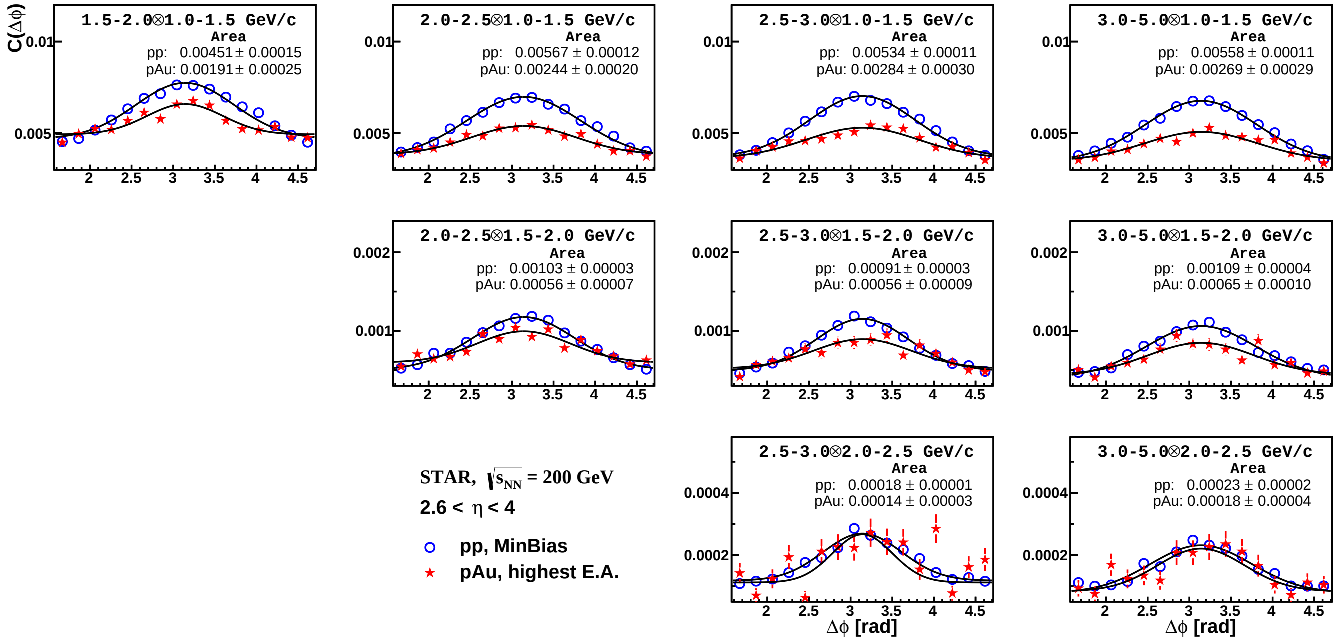

FIG. 1. (color online). The forward ($2.6 < \eta < 4.0$) back-to-back di-π^0 correlations in MinBias p+p and the highest event activity p+Au collisions for various p_T ranges. The value for the area of the peak obtained from the Gaussian fit is given in each panel.

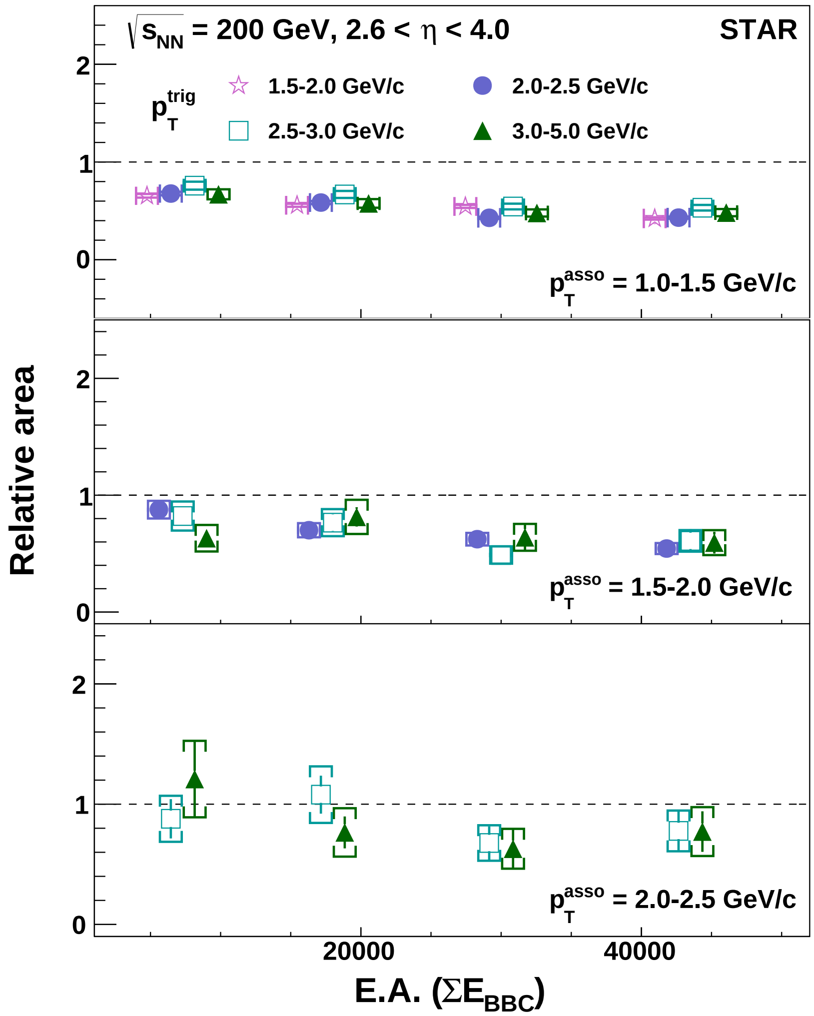

FIG. 2. (color online). The area of forward ($2.6 < \eta < 4.0$) back-to-back di-π^0 correlations in different event activity p+Au classes relative to the area in MinBias p+p collisions for various p_T ranges. The vertical bars indicate the sizes of the statistical uncertainties and the horizontal brackets indicate the sizes of the point-to-point systematic uncertainties. Some data points have been offset horizontally to improve figure clarity.

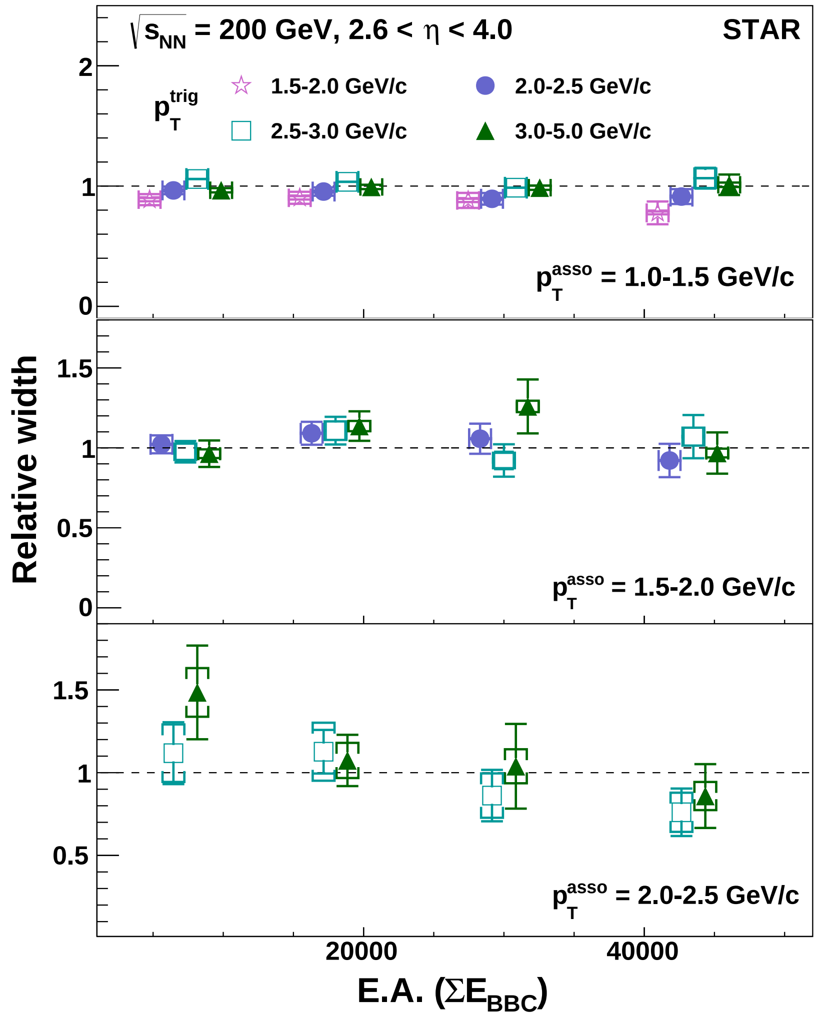

FIG. 3. (color online). The width of forward ($2.6 < \eta < 4.0$) back-to-back di-π^0 correlations in different event activity p+Au classes relative to the width in MinBias p+p collisions for various p_T ranges. The vertical bars indicate the sizes of the statistical uncertainties and the horizontal brackets indicate the sizes of the point-to-point systematic uncertainties. Some data points have been offset horizontally to improve figure clarity.

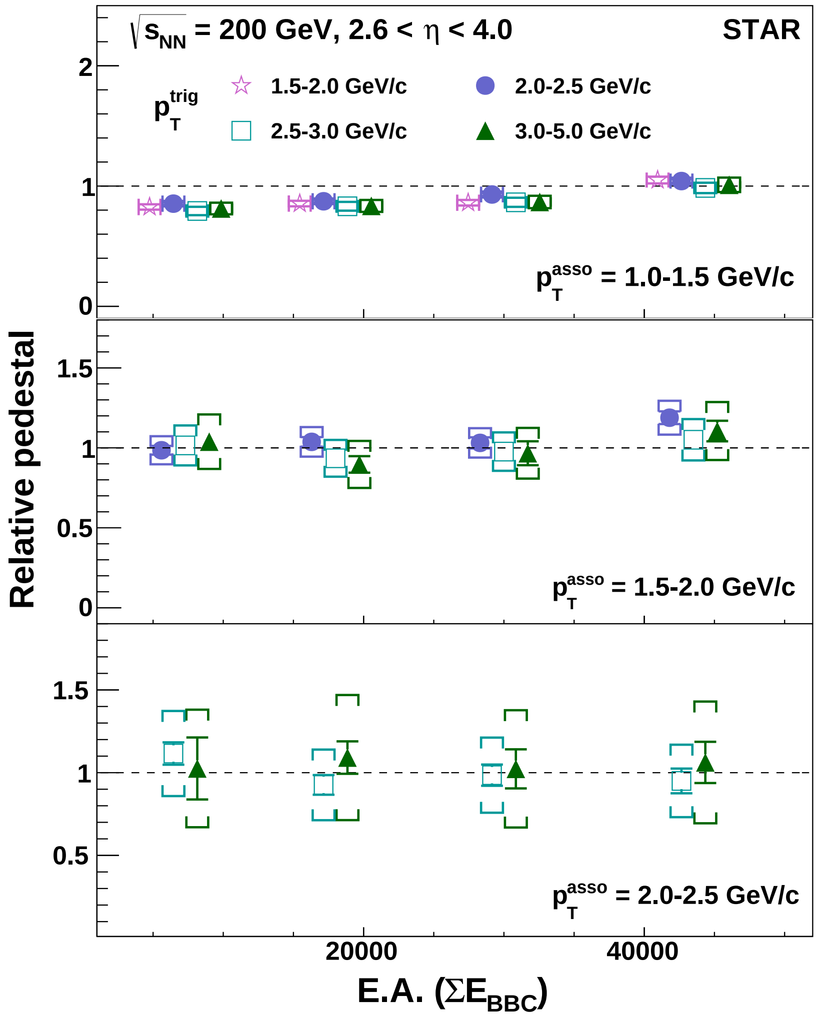

FIG. 4. (color online). The pedestal in forward ($2.6 < \eta < 4.0$) back-to-back di-π^0 correlations in different event activity p+Au classes relative to the pedestal in MinBias p+p collisions for various p_T ranges. The vertical bars indicate the sizes of the statistical uncertainties and the horizontal brackets indicate the sizes of the point-to-point systematic uncertainties. Some data points have been offset horizontally to improve figure clarity.

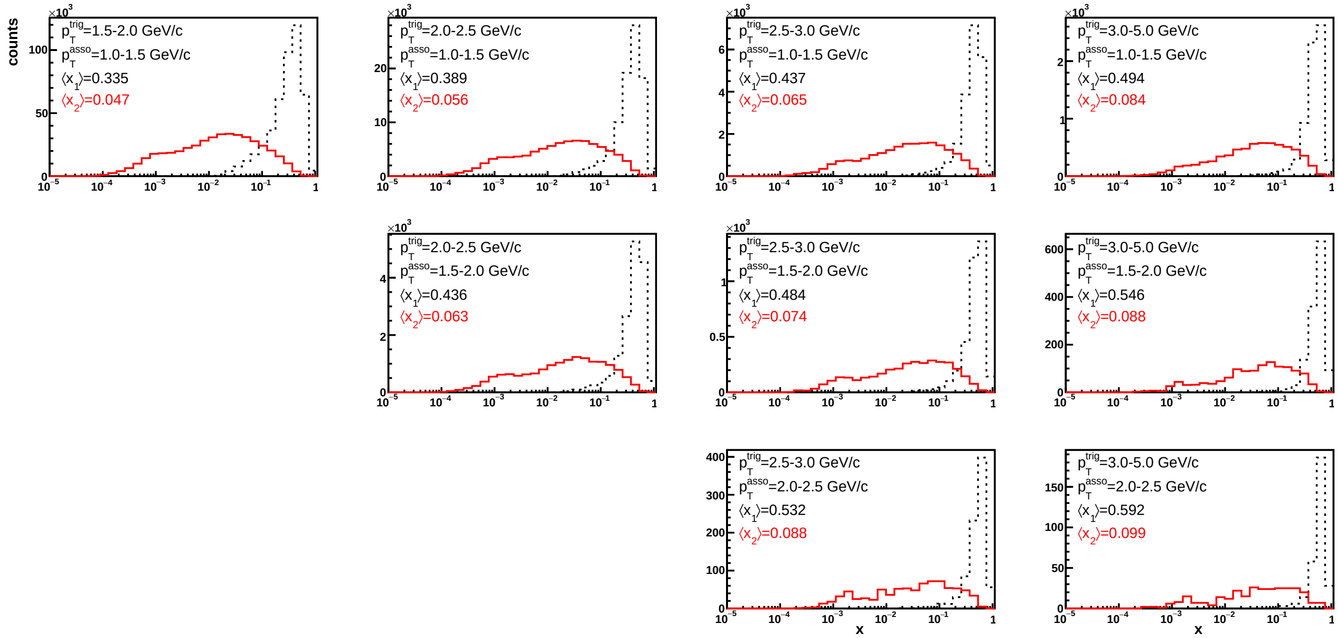

FIG. 5. (color online). Monte Carlo simulations of x_1 and x_2 distributions in various p_T ranges for $pp \to \pi^0\pi^0$X collisions at $\sqrt{s_{\rm NN}}$ = 200 GeV. The pseudorapidity range of the outgoing π^0s is from 2.6 to 4. The mean values of x_1 and x_2 are given in each panel

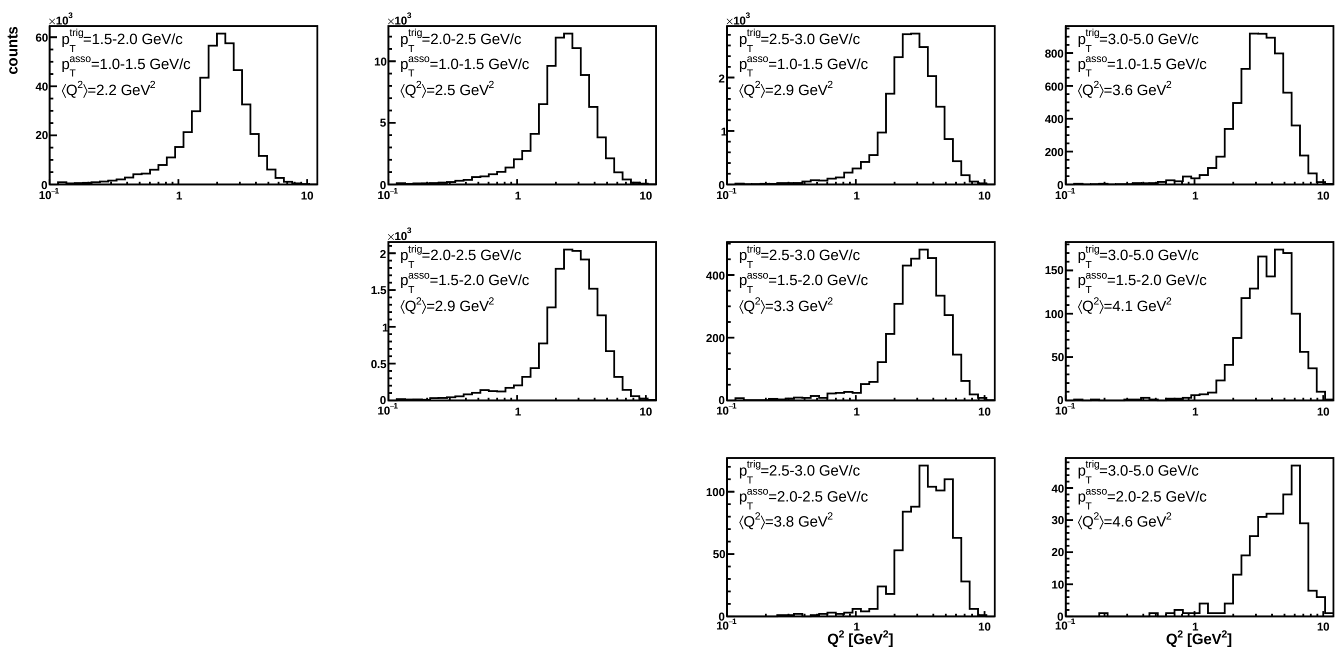

FIG. 6. Monte Carlo simulations of Q^2 in various p_T ranges for $pp \to \pi^0\pi^0$X collisions at $\sqrt{s_{\rm NN}}$ = 200 GeV. The pseudorapidity range of the outgoing π^0s is from 2.6 to 4. The mean value of Q^2 is given in each panel.